



OPEN ACCESS

EDITED BY

Jingbin Wang,
SINOPEC Petroleum Exploration and
Production Research Institute, China

REVIEWED BY

Jianglin He,
China Geological Survey, China
Xiaoqi Wu,
SINOPEC Petroleum Exploration and
Production Research Institute, China

*CORRESPONDENCE

Lixia Liao,
✉ 909051757@qq.com
Jianda Liu,
✉ 13505181390@163.com

RECEIVED 14 August 2023

ACCEPTED 08 September 2023

PUBLISHED 25 September 2023

CITATION

Liao L, Zhou Y, Lin Z, Wang X, Chen W,
Li J, Zheng C, Yu W, Li X and Liu J (2023),
Gas geochemistry of the hot springs gas
in Fujian province, SE China: insight into
the deep faults and seismic activity.
Front. Earth Sci. 11:1277100.
doi: 10.3389/feart.2023.1277100

COPYRIGHT

© 2023 Liao, Zhou, Lin, Wang, Chen, Li,
Zheng, Yu, Li and Liu. This is an open-
access article distributed under the terms
of the [Creative Commons Attribution
License \(CC BY\)](https://creativecommons.org/licenses/by/4.0/). The use, distribution or
reproduction in other forums is
permitted, provided the original author(s)
and the copyright owner(s) are credited
and that the original publication in this
journal is cited, in accordance with
accepted academic practice. No use,
distribution or reproduction is permitted
which does not comply with these terms.

Gas geochemistry of the hot springs gas in Fujian province, SE China: insight into the deep faults and seismic activity

Lixia Liao^{1*}, Yueyong Zhou¹, Zhiying Lin¹, Xiaowei Wang¹,
Wei Chen¹, Jiyu Li¹, Chenhe Zheng¹, Wenjun Yu¹, Xingmei Li¹ and
Jianda Liu^{2*}

¹Fujian Earthquake Agency, Fuzhou, China, ²Jiangsu Earthquake Agency, Nanjing, China

Fujian province is located at the forefront of the South China continental margin, situated on the edge of the Circum-Pacific seismic belt, and it is one of the regions with the most active neotectonic and geothermal activities in Chinese mainland. To explore the geochemical signals of hot spring gases to tectonic activity and earthquakes, a collection of geothermal gas samples was collected from 29 locations in Fujian from January 2021 to December 2022 (many of which were multiply collected at several sites quarterly). The gas samples were tested for their gas composition, helium, neon, carbon isotopes, radon contents, and gas flow rates. The results show that the dominant component of the hot spring outgassing is N₂, and the increase in CO₂ content is often associated with the increasing ¹³C. The variation range of the helium isotope ratio (³He/⁴He) in the hot spring gases is between 0.06 and 2.20Ra, and Rc/Ra varies between 0.06 and 1.58, with peak values occurring at the intersections of deep faults. Radon contents range from 18 to 2000 Bq/L. Calculations revealed that the maximum proportion of mantle-derived helium is 30.2%, and the mantle-derived heat contribution ranges from 37.6% to 63.4%. These data indicate a significant mantle degassing process in Fujian, with a high degree of mantle-crust connectivity, and mantle-derived heat as the main source of geothermal activity in the area. Comparative analysis with regional seismic activity indicates that areas with relatively strong upwelling of deep fluids are the main regions of regional seismic activity, and seismic intensity is positively correlated with mantle-derived heat flow. Thus, deep thermal fluid actives are closely genetically correlated to regional seismic activity. Additionally, the correlation analysis with the Taiwan M_{L6.0} earthquake suggests that high ³He/⁴He, δ¹³C_{CO2} values of hot spring gas and gas flow velocity in Nancheng Hot Spring (QZ6) indicate significant short-term and imminent anomaly indications preceding M_{L6.0} earthquakes in the Taiwan region.

KEYWORDS

gas geochemistry, He isotope, hot spring, mantle thermal convection, seismic activity

1 Introduction

Hot spring gases originate from deep Earth and are less affected by near-surface hydrological processes, making them capable of carrying more direct information about deep geological environments (Lowenstern et al., 2015). Compared to soil gases, hot spring gases are less vulnerable to atmospheric contamination (Sugisaki et al., 1982). As a result,

since the beginning of this century, it has received increasing attention and applications. They have been applied in determining geothermal systems, such as identifying volcanic geothermal systems (Giggenbach et al., 2001) or magma heat source geothermal systems (Guo, 2022), identification of controlling structures (Fridriksson et al., 2016; Marco et al., 2021; Zhang et al., 2021), estimation of terrestrial heat flow (Polyak et al., 1979; Wang, 1999), inferring the temperatures of strata at certain depths (Duchkov et al., 2010), determining the age of geothermal water (Torgersen and Stute, 2013; Li et al., 2017). Additionally, the isotopic compositions of hot spring gases have been used to trace the material source and deep transport mechanisms of geothermal gases (Sano and Marty, 1995; Arnórsson, 2000; Pinti et al., 2013). In recent years, they have been increasingly applied to investigate active fault structures, and seismic activity (Wakita and Nakamura, 1980; Italiano et al., 2010; Chen et al., 2015; Zhou et al., 2017).

Fujian Province is located at the southeastern edge of the Eurasian continent and falls within the Circum-Pacific geothermal belt, Adjacent to the Ryukyu Islands subduction zone - Taiwan Island arc collision zone between the Philippine Sea plate and the Eurasian plate. Taiwan is one of the most seismically active regions in the world, and strong plate margin subduction has formed a high-temperature geothermal anomaly area here. Due to its unique tectonic position, Fujian has become one of the provinces with the most active tectonic and geothermal activities on the Chinese mainland. It ranks the third in density of hot spring in China (Zhuan, 2015), providing important insights into the deep faults and seismic activities. The current consensus suggests that the hot springs in Fujian are a convection-type geothermal system formed by deep circulation of atmospheric precipitation. The NE-trending faults are recognized as heat-controlling structures (Cheng, 1992; Zhuan, 2010; Tian et al., 2021a). However, there is no unified understanding of the heat source, with some proposing that the main heat source of the hot springs is from post-Quaternary intrusive magmatic heat (He and Chen, 1999) or the heat generated by U, Th, and K (Cheng et al., 2021), while others suggest a combination of these heat sources, with mantle-derived heat considered insignificant.

In the past 2 years, we have conducted continuous sampling and observation of the outgassing of hot springs, thermal water boreholes, and cold springs in Fujian for analyses of He-Ne-C isotopes and gas volume percentages as well as on-site observations of radon gas, gas flow rates, and water temperatures. In this paper, we present the chemical compositions and He-Ne-C isotope variations of representative samples from hot spring gas boreholes, as well as the dynamic characteristics of hot spring gas flow rates, and aim to reveal the influence of regional tectonics on geothermal sources and heat-controlled structures. Furthermore, our studies provide essential evidence for the existence of widespread mantle convective heating, multiple mantle diapir, Moho dislocation structures in Fujian, and predictions of seismic activity in the Taiwan region.

2 Geological setting

Fujian Province is situated on the southeastern edge of the Asian continent, located within the tectonic contact zone between the

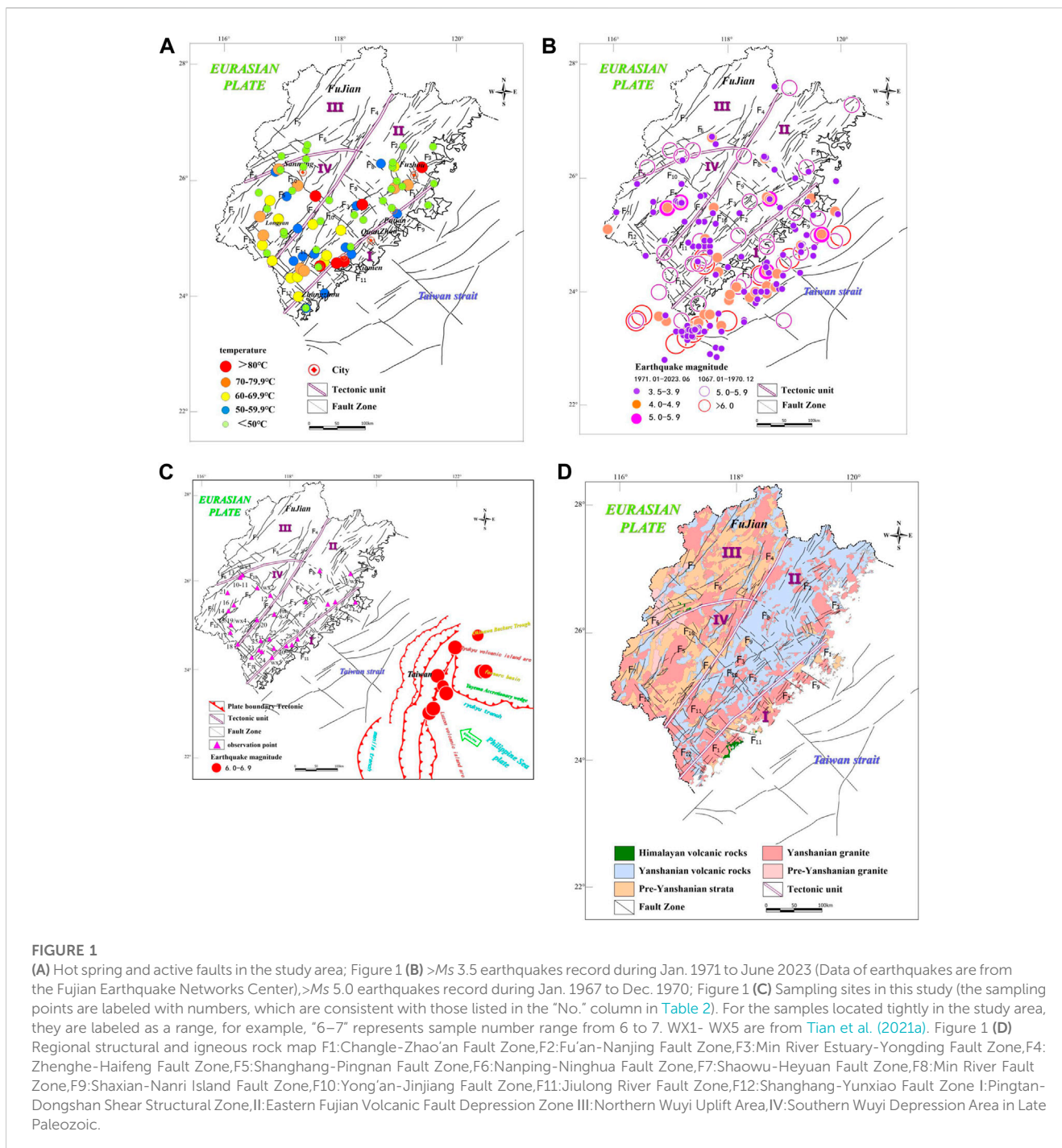
Eurasian and Philippine Sea Plates. Influenced by the Mesozoic Pacific subduction plate, the region has developed a series of approximately parallel NNE-trending deep faults and NW-trending transtensional faults, which together form a chessboard-like structural pattern (see Figure 1A). Along with the uplifting of the crust and multiple large-scale Mesozoic intermediate-acidic magma intrusions and volcanic eruptions, a series of faulted basins have formed along the NNE and NWW structures, creating favorable conditions for the occurrence of geothermal resources. The area of the outcropping igneous rocks in the entire region is approximately $8 \times 10^4 \text{ km}^2$, accounting for two-thirds of the total land area of the province. Most of the province's hot springs and geothermal resources are related to the faults and fracture systems associated with the Yanshanian granite, belonging to the fissure-type belt-like geothermal reservoirs (Zhuan, 2015).

Most of the NE-trending faults are deep-seated and serve as boundaries for tectonic units. For instance, the Zhenghe-Haifeng fault zone (F4) acts as the boundary between the Huaxia block in western Fujian and the Mesozoic magmatic belt along the southeastern coast. The Changle- Zhao'an fault zone (F1) in the eastern region marks the boundary between the Pingtan-Dongshan shear Structural Zone (I) and the Eastern Fujian Volcanic Fault Depression Zone (II). In the western part, the Nanping-Ninghua fault zone (F6) acts as the boundary between the Northern Wuyi Uplift Area (III) and the Southern Wuyi Depression Area in Late Paleozoic (IV) (Geology investigation institute of Fujian province, 2016). The Mindong volcanic faulted zone is characterized by large-scale Mesozoic volcanic eruptions.

Hot springs mainly develop along these fault zones, particularly at intersections of different-trending faults. Hot springs are highly abundant along the Fu'an-Nanjing fault zone. This fault zone is the site of Huangchulin (FZ1) hot spring, where it intersects with the F8 fault of the Min River fault zone. The well-known Zhangzhou thermal field is present in the Zhangzhou area. At the intersection of the Fu'an-Nanjing fault zone (F2) and the NW-trending Jiulong River fault zone (F11), there are Hua'an tainei (ZZ22) hot spring, ZZ23, ZZ24, and other hot springs. At the intersection with the Min River Estuary- Yongding fault zone, there is the Shiniushan volcano edifice, where there is Nancheng Hot Spring (QZ6) with the highest spring temperature in eastern China, 89°C. At the intersection of the Jiulong River fault zone with the Changle- Zhao'an fault zone, the highest borehole temperature in eastern China, 121.5°C, is recorded at the Gongren Sanatorium Well (sampling was not possible due to ongoing blowouts).

3 Sampling and methods

In this study, geothermal gas samples were collected from 29 locations, including natural springs, wells, and one cold spring outgassing, with specific locations shown in Figure 1C. For bubbling springs and artesian wells (with water flowing upward), a water drainage and gas collection method were used. A 500-mL glass bottle with a polytetrafluoroethylene funnel attached to its mouth was filled with hot spring water and inverted under the water surface to immerse it in the geothermal spring. For non-artesian wells, hot water was pumped for 20 min and filled into a bucket. Then, a glass



bottle filled with hot spring water was submerged in the water, with the funnel aligned with the rising water flow in the bucket. Approximately two-thirds of the glass bottle volume was filled with gas before sealing it with a rubber cap to avoid atmospheric contamination. Each sampling point collected two parallel samples, one for determining the $^3\text{He}/^4\text{He}$ and $^4\text{He}/^{20}\text{Ne}$ ratios and the other for $\delta^{13}\text{C}_{\text{V-PDB}}(\text{CO}_2)$ values. For some potential hot spring sites with preliminary evaluations of seismic monitoring value, multiple samples and observations were conducted at 3-month intervals, along with additional gas component observations. Furthermore, since January 2021, continuous observations of QZ6 gas flow rates

have been carried out every 3 days using the same method as gas sampling, employing an emptying approach. The time taken to evacuate the hot spring water from the glass bottle was recorded using a stopwatch, and subsequent calculations were performed. An empirical threshold (The upper limit value is 0.543 mL/s, and the lower limit value is 0.173 mL/s) was established to determine data anomalies. Values exceeding this threshold were considered as anomalies, and the principle for defining these anomalies was based on their association with the highest number of seismic events.

In-situ observations of radon outgassing were conducted using an Alpha-GUARD P2000-series radon detector. The

TABLE 1 Chemical composition of hydrothermal volatiles from Fujiang of China in this study ("—" represents no analysis, "-" represents the content lower than the detection limit 0.0001%).

Location	No	Latitude N (°)	Longitude E (°)	N ₂	CO ₂	CH ₄	O ₂	Ar	He	H ₂	CO	C ₂ H ₆	C ₃ H ₈
Fuzhou	FZ1	26.2801	118.7022	89.31	6.25	0.03	3.09	1.12	0.2000	-	-	-	-
	FZ2	25.5604	119.5201	96.60	0.05	0.07	1.84	1.14	0.3050	0.0008	-	-	-
	FZ3	26.2139	119.4104	—	—	—	—	—	—	—	—	—	—
	WX1	26.2142	119.4102	95.77	0.13	0.08	0.53	1.72	0.2491	0.0018	-	-	-
Putian	PT4	25.5684	119.0605	98.15	0.18	0.00	0.45	1.16	0.0565	-	-	-	-
	PT5	25.512	118.8902	—	—	—	—	—	—	—	—	—	—
	QZ6	25.5699	118.3796	95.07	0.91	0.77	1.14	1.72	0.3540	0.0035	0.0003	0.0004	0.0005
Quanzhou	QZ7	25.567	118.3849	—	—	—	—	—	—	—	—	—	—
	QZ8	25.2816	117.6631	—	—	—	—	—	—	—	—	—	—
	QZ9	25.2826	117.6632	—	—	—	—	—	—	—	—	—	—
Sanming	SM10	26.1804	116.9373	92.19	3.03	1.20	1.55	1.48	0.5580	0.0003	-	-	-
	SM11	26.1803	116.9366	—	—	—	—	—	—	—	—	—	—
	SM12	25.7171	117.5762	84.76	6.27	0.00	7.61	1.24	0.1123	-	-	-	-
	SM13	26.1341	116.8819	—	—	—	—	—	—	—	—	—	—
	WX2	25.8925	117.2745	19.22	75.65	0.04	1.69	0.21	0.0484	0.0001	-	-	-
	WX3	26.1306	116.8866	92.59	4.90	0.34	0.52	1.22	0.7098	0.0001	-	-	-
Longyan	LY14	25.3616	116.6139	67.42	25.83	0.18	5.23	1.03	0.3060	0.0010	0.0003	0.0001	0.0002
	LY15	25.0403	116.6739	89.05	6.89	0.03	2.31	1.27	0.4420	0.0001	-	-	-
	LY16	25.4965	116.7398	80.35	17.96	0.01	0.54	1.02	0.1176	-	-	-	-
	LY17	24.8672	116.656	96.07	0.12	0.09	2.26	1.26	0.2200	-	-	-	-
	LY18	24.5985	116.8286	—	—	—	—	—	—	—	—	—	—
	LY19	25.0398	116.6727	—	—	—	—	—	—	—	—	—	—
	LY20	25.15556	117.2682	—	—	—	—	—	—	—	—	—	—
	LY21	25.7765	116.5972	—	—	—	—	—	—	—	—	—	—
	WX4	25.0403	116.6739	94.30	2.28	0.04	1.14	1.14	0.4599	0.0001	-	-	-
Zhangzhou	ZZ22	24.7169	117.5543	97.25	0.60	0.21	0.50	1.31	0.1343	0.0003	-	-	-
	ZZ23	24.4639	117.3162	95.85	0.03	0.15	2.30	1.47	0.2067	-	-	-	-
	ZZ24	24.4253	117.3799	96.82	0.12	0.13	1.35	1.41	0.1667	0.0007	-	-	-
	ZZ25	24.676	117.3537	—	—	—	—	—	—	—	—	—	—
	ZZ26	24.2994	117.1487	—	—	—	—	—	—	—	—	—	—
	WX5	25.3616	116.6139	97.28	0.15	0.03	0.64	1.44	0.1523	0.0012	-	-	-
Xiamen	XM27	24.5594	117.9405	97.01	0.45	0.07	0.93	1.38	0.1600	0.0059	-	-	-
	XM28	24.584	118.0661	88.69	7.07	0.14	2.62	1.35	0.1195	0.0230	-	-	-
	XM29	24.7134	118.195	—	—	—	—	—	—	—	—	—	—

detection limit of the instrument is 1Bq/m³, and the upper limit is 2000 Bq/m³. All samples were analyzed within half a month after field investigations in the Key Laboratory of Petroleum Resources of the Northwest Institute of Eco-Environment and Resources, Chinese Academy of Sciences. The ³He/⁴He and ⁴He/²⁰Ne ratios

were analyzed using a Noblesse noble gas mass spectrometer produced by Nu Instruments, United Kingdom. Gas compositions were determined using a mass spectrometer MAT 271 with relative standard deviations of less than 5%. The detection limit is 0.0001%. The δ¹³CV-PDB (CO₂) values

TABLE 2 Isotopic composition of hydrothermal volatiles in this study area ("—" represents no analysis, "\leq" represents the content lower than the detection limit, "aq" represents Radon dissolved in water).

No	T (°C)	Rn (Bq/L)	⁴ He/ ²⁰ Ne	R/Ra	Rc/Ra	Mantle derived helium (%)	δ ¹³ C _{CO2}	q (mW/m ²)	q _m (mW/m ²)	q _c (mW/m ²)	q _m /q (%)
FZ1	52.3	510*	196	1.58	1.58	19.8	-12.5	78.7	46.9	31.8	60
FZ2	42.5	15	193	0.59	0.59	7.4	-18.9	70.9	35.9	35.0	51
FZ3	82.5	28*	89	0.50	0.50	6.2	-19.1	69.6	34.4	35.2	49
WX1	81	—	109	0.35	0.35	4.4	—	66.7	31.3	35.4	47
PT4	49.1	419	29	0.18	0.17	2.1	-23.8	61.0	26.0	35.0	43
PT5	33	69*	59	0.24	0.24	3.0	-18.1	63.7	28.4	35.3	45
QZ6	89.8	—	216	0.25	0.25	3.1	-13.7	64.1	28.7	35.3	45
QZ7	94.1	2,100	105	0.27	0.26	3.3	-13.1	64.4	29.0	35.4	45
QZ8	44.5	—	71	0.09	0.08	1.1	-21.5	55.0	21.4	33.6	39
QZ9	34.5	—	96	0.07	0.07	0.8	-22.1	54.0	20.7	33.3	38
SM10	77.7	1789	341	0.34	0.34	4.3	-14.2	66.5	31.1	35.4	47
SM11	78.7	—	372	0.35	0.35	4.4	-14.0	66.7	31.3	35.4	47
SM12	70.2	98	71	1.12	1.12	14.0	-13.5	75.9	42.6	33.3	56
SM13	55.9	185*	464	0.44	0.44	5.5	-10.9	68.5	33.3	35.3	49
WX2	72	—	162	1.28	1.28	16.1	-6.7	77.0	44.2	32.8	57
WX3	54	—	408	0.41	0.41	5.1	-12.1	68.0	32.6	35.3	48
WX4	68	—	265	1.10	1.10	13.8	—	75.8	42.4	33.4	56
LY14	71.5	210	308	1.65	1.65	20.7	-8.6	79.0	47.5	31.5	60
LY15	69.4	488	305	1.45	1.22	15.3	-11.4	76.6	43.6	33.0	57
LY16	34.7	14*	78	2.19	2.20	27.6	-10.3	81.3	51.5	29.8	63
LY17	60.2	32	171	0.83	0.83	10.4	-15.3	73.6	39.3	34.2	53
LY18	60.1	120*	94	0.07	0.06	0.8	-17.7	52.8	19.8	32.9	38
LY19	74.7	—	315	1.36	1.36	17.0	-10.8	77.5	45.0	32.5	58
LY20	58.9	301	51	0.24	0.24	3.0	-19.2	63.7	28.4	35.3	45
LY21	19.1	-	0.58	1.49	2.08	26.1	-16.3	80.8	50.7	30.2	63
ZZ22	58.1	68*	73	0.36	0.36	4.5	-19.2	67.0	31.6	35.4	47
ZZ23	75.9	358	126	1.08	1.08	13.5	-12.3	75.7	42.2	33.4	56
WX5	70	—	73	1.39	1.39	17.4	-15.4	77.6	45.2	32.4	58
ZZ24	71.8	51	92	0.82	0.82	10.2	-17.0	73.5	39.2	34.3	53
ZZ25	54.2	93*	79	0.35	0.35	4.35	-18.1	66.7	31.3	35.4	47
ZZ26	61	72*	31	0.53	0.53	6.6	-17.4	70.0	34.9	35.1	50
XM27	82	104	77	0.24	0.24	3.0	-16.3	63.7	28.4	35.3	45
XM28	89.2	148	87	0.19	0.19	2.3	-16.0	61.9	26.8	35.1	43
XM29	53.8	65	153	0.59	0.59	7.4	-22.5	70.9	35.9	35.0	51

were determined using the MAT253 isotope ratio mass spectrometer. The conventional delta notation per mil (‰) expressed the C isotopic ratios following the Pee Dee

Belemnite (PDB) from South Carolina. The measurement errors for carbon isotopic ratios were ±0.2‰, and the analytical precision of δ¹³C was 0.3‰ (Tian et al., 2021a).

4 Results

4.1 Components of gases

The observation results of gas components for 15 hot spring outgassing sites (Table 1) indicate that N₂ is the dominant component of hot spring outgassing, and accounts for 67.42%–98.15% of the total volume, with 60% of the gas samples having N₂ vol% exceeding 90%. Other gases include varying amounts of CO₂, O₂, Ar, He, CH₄, and other trace gases, such as H₂. Some individual measurement points detect trace amounts of CO, C₂H₆, C₃H₈, H₂S, and H₂. The volume percentages of CH₄ and H₂ are both below 1.20% and 0.0230%, respectively. CO₂ content in the study area varies, with LY14 and LY16 having relatively high contents of 25.83 vol% and 17.96 vol%, respectively, while other measurement points range from 0.03% to 7.07%. The noble gas, argon (Ar), ranges from 1.02% to 1.72%, and helium (He) content is between 0.0565% and 0.5580%, both of which are less than 1%. The O₂ content in hot spring outgassing varies from 0.45% to 7.61%. However, due to the potential atmospheric contamination during the sampling and analysis process and the possibility of atmospheric mixing during the transportation of deep-seated gases to the surface, these O₂ content values may not accurately represent the actual overflow gas content of the hot springs.

4.2 Isotopes, radon, and gas flow rates

To assess the level of air pollution, the parameter ⁴He/²⁰Ne ratio is introduced. ²⁰Ne originates from the atmosphere, and the ⁴He/²⁰Ne ratio in the atmosphere is 0.318 (Sano and Wakita, 1985). In this study, the ⁴He/²⁰Ne sample ratio for hot spring outgassing ranges from 29 to 464, significantly higher than the atmospheric value of 0.318, indicating that atmospheric contamination during sampling and isotopic measurements is minimal or negligible. To correct for this atmospheric contamination, the method and calculation formula proposed by Craig et al. (1978) for atmospheric correction of helium isotopic composition were used to correct the measured ³He/⁴He ratio (R_c). The corrected ³He/⁴He ratios range from 0.07 to 2.20 R_a. The δ¹³C values (relative to PDB) of CO₂ in the samples range from –22.5‰ to –8.7‰. *In-situ* observations of radon concentration range from 18 to 2000 Bq/L. However, since the instrument's detection limit is 2000 Bq/L, the actual radon content for QZ7, which exceeds the detection limit, should be higher than 2000 Bq/L (Refer to Table 2 for details). QZ6 gas flow rate observations show dynamic fluctuations around the mean line, ranging from 0.14 to 0.97 mL/s, with most values around 0.38. Peak values occur on 2021-03-28, 2022-01-04, 2022-03-02, 2022-05-07, 2022-05-22, and 2022-07-12, while low values occur on 2021-10-10 and 2021-07-20 (Figure 9).

5 Discussion

5.1 Sources of He and CO₂

5.1.1 Helium

In natural gas reservoirs, the concentration of atmospheric helium is negligible, hence it is not necessary to consider its

atmospheric contribution. Therefore, a binary composite model can be used to calculate the proportions of crustal and mantle helium components in natural gas samples. The contribution of mantle source He can be calculated as follows as follows (Xu, 1997):

$$\frac{(^3\text{He}/^4\text{He})_S - (^3\text{He}/^4\text{He})_C}{(^3\text{He}/^4\text{He})_M - (^3\text{He}/^4\text{He})_C} \times 100$$

Where C represents the crustal source, S represents the atmospheric source, and M represents the mantle source. The results estimated using a binary mixing model indicate that, except for two samples contaminated by 1%, air pollution during the sampling was less than 1%. In the Fujian region, the mantle-derived helium component in the remaining 33 hot spring gas samples ranges from 0.77% to 27.55%, suggesting that helium in hot spring gases mainly originates from the crust, but there is still some contribution from the mantle. Figure 2 and Table 2 show that, except for samples 8, 9, and 18 with mantle-derived helium at around 1%, almost all other samples have a certain proportion of mantle-derived helium. Among them, 12 hot spring gas samples, such as samples numbered 16, 14, 1, WX5, 19, WX2, 15, 23, 12, 24, WX4, and 17, exhibit significant mantle-derived helium, accounting for more than 10% of the composition. Additionally, 6 hot spring gas samples, including samples numbered 29, 2, 26, 3, 13, and WX3, have a small amount of mantle-derived helium, accounting for 5%–10% of the composition. It is worth noting that the proportion of mantle-derived helium exceeding 5% accounts for 54.55% of all samples, indicating that the presence of mantle-derived helium in hot spring gases is common in the Fujian region. This is significantly different from cratonic basins (Ordos, Sichuan, and Tarim) in China, where the helium is thought to be of typical crustal origin with R/R_a<0.24 (Dai et al., 2022; Liu et al., 2022; Peng et al., 2022). In Chinese mainland, mantle-derived helium is commonly found in volcano areas and continental rifts, such as the Tengchong volcanic region in Yunnan province, SW China. Due to the strong compression and subduction of the Indian Plate towards the Eurasian Plate, numerous fault zones have formed in the Tengchong volcano region, which contains over 70 Quaternary volcanoes with widespread hot springs. The ³He/⁴He values of degassed spring waters range from 3.21×10^{–6} to 7.18×10^{–6}, represented by R/R_a values of 2.29–5.1, estimating the mantle-derived helium component to be between 29% and 65% (Wang PZ. et al., 1993). Another source of mantle-derived helium occurs in the eastern continental rifts of China, where there are numerous upper mantle-derived basaltic rocks, and intense ancient volcanic activity. There exist anomalous mantle layers beneath the crust, and the crust is stretched and thinned by the upwelling mantle, leading to the upward escape of fluids. Helium isotope geochemical data suggest that the eastern continental rifts of China have been in a state of strong degassing of the upper mantle since the late Tertiary, with active Mesozoic and Cenozoic tectonic activities and frequent magmatic activities. Taking the Tan-Lu fault zone as an example, it is a super-crustal fault that deeply cuts through the mantle, providing a channel for the transportation of mantle-derived volatile components to the sedimentary crust. The distribution of high ³He/⁴He values is related to this tectonic environment, and the mantle-derived helium component can reach 33.5%–65.4% (Du et al., 1994; Xu, 1996). Because Fujian province does not have

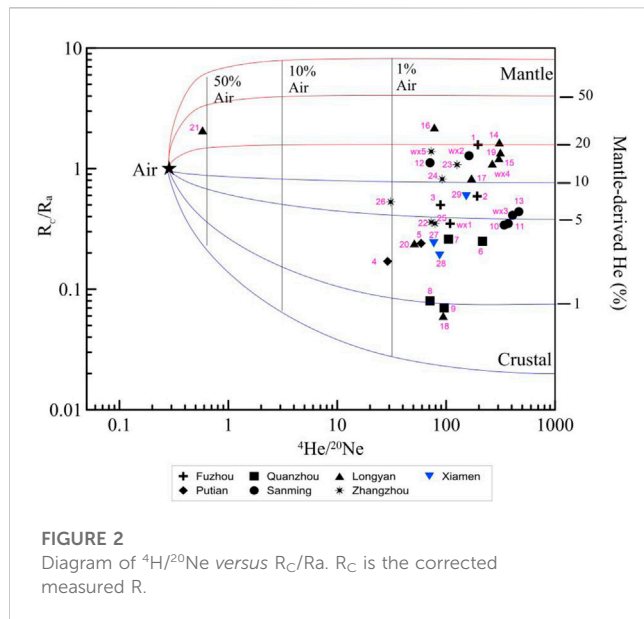


FIGURE 2
Diagram of $^4\text{H}/^{20}\text{Ne}$ versus R_c/R_a . R_c is the corrected measured R .

active Quaternary volcanoes, it is unlikely for mantle-derived helium to be released in volcanic regions. On the other hand, Fujian province is located in the junctional zone between the Eurasian and Philippine Sea plates, in the southeastern part of China. Previous isothermal Curie point, microseismic, and artificial seismic detection data have revealed the existence of a low-velocity layer and deep large faults cutting into the mantle in the region (Wei et al., 1988; Ma, 2002). Based on this, it can be inferred that mantle-derived helium is transported to the surface through deep-seated super-crustal faults, assisted by deep circulating hot springs, in Fujian (Figure 8). The deep fault system is the key factor exerting control on the migration and accumulation of mantle-derived helium-rich fluids (Wang et al., 2023).

5.1.2 CO_2

The CO_2 in natural is mostly of typical crustal origin (Wu et al., 2013; Liu et al., 2018). The sources of CO_2 in hot spring gases can be mainly classified into three endmembers: mantle-derived, organic, and metamorphic inorganic sources. The recognized range of $\delta^{13}\text{C}$ values for mantle-derived carbon is between -8‰ and -5‰ (Javoy et al., 1986), with the lower limit of -8‰ used as the endmember value. Organic-derived CO_2 typically has $\delta^{13}\text{C}_{\text{CO}_2}$ values below -10‰ , while biological CO_2 is marked by low $\delta^{13}\text{C}_{\text{CO}_2}$ values ranging from -70‰ to -25‰ (using the upper limit of -25‰ as the endmember value for organic carbon). Inorganic-derived CO_2 generally exhibits $\delta^{13}\text{C}$ values heavier than -8‰ , and the $\delta^{13}\text{C}$ value for metamorphic carbonate-derived CO_2 is close to 0‰ (Faure et al., 1965; Dai, 1993; Sano and Marty, 1995) (using 0‰ as the endmember value for metamorphic inorganic-derived carbon, Draw a three terminal diagram, as shown in Figure 3). As the carbon isotopes of CO_2 from various sources in hot spring gases overlap, it is not possible to directly determine the main source of CO_2 based solely on carbon isotopes (Zhou et al., 2020). Therefore, when attributing the origin of certain components in hot spring gases, a comprehensive analysis using multiple indicators is considered more reliable than relying on a single indicator. By conducting integrated analyses, it is found that

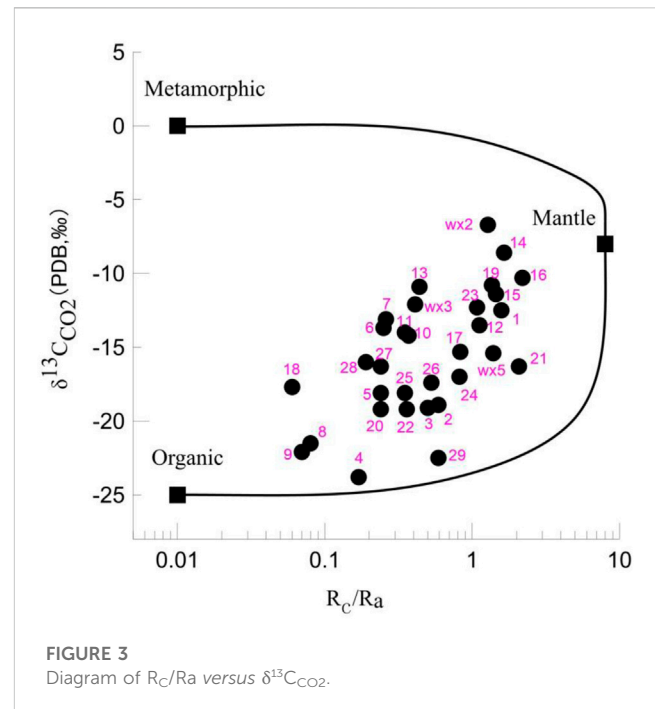
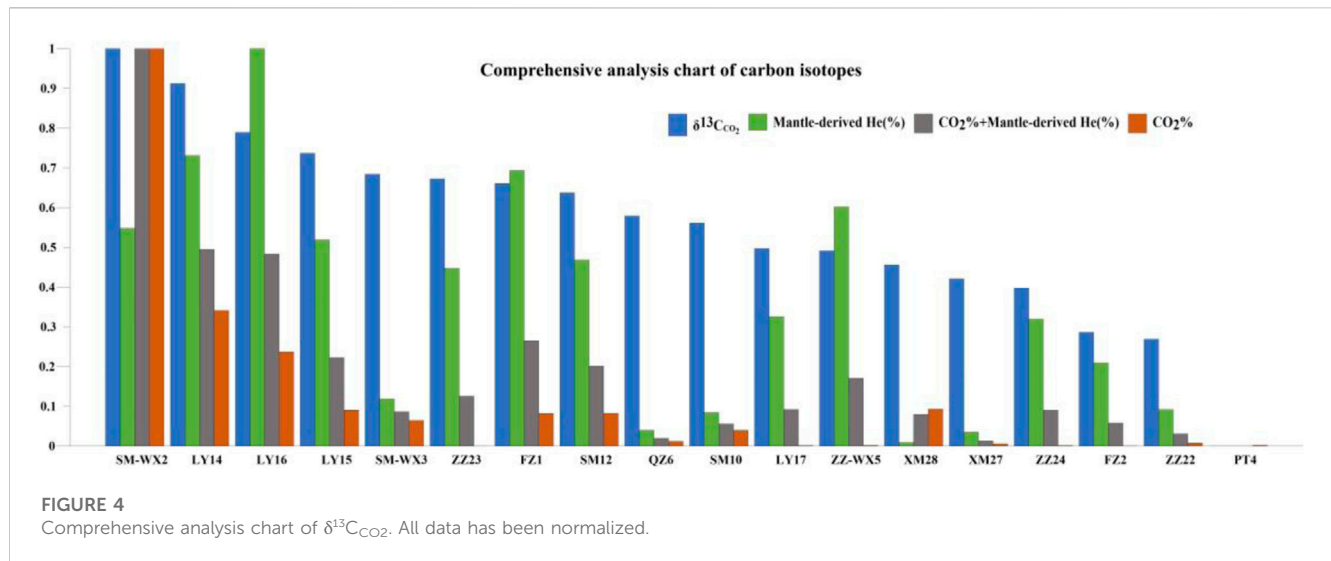


FIGURE 3
Diagram of R_c/R_a versus $\delta^{13}\text{C}_{\text{CO}_2}$.

the increase in $\text{CO}_2\%$ content is accompanied by the enrichment of ^{13}C isotopes, as shown in Figure 4. This enrichment can be attributed to the metamorphism processes of carbonate rocks in the deep crust. Analyzing the combined data from Figure 2 and 3, it is observed that samples with mantle-derived helium concentrations exceeding 10% (e.g., WX2, 16, 14, 19, 15, 1, 12) in Figure 2 are still positioned close to the mantle in Figure 3. This suggests that the high ^{13}C values in WX2, 16, 14, 19, 15, 1, and 12 are not solely formed due to metamorphic processes but are jointly influenced by metamorphic and mantle sources. From the perspective of CO_2 content, sample 23 in Figure 4 does not follow the trend of increased CO_2 content associated with ^{13}C isotope enrichment. Even though it does not have a high CO_2 , its $\delta^{13}\text{C}$ value is relatively high and ranks higher. This implies that the contribution rate of mantle-derived $\delta^{13}\text{C}$ is higher at this sampling point, suggesting the presence of deep-seated fault systems. In fact, sample 23 does have high mantle-derived helium (Figure 2), and geophysical data also indicate the presence of deep-seated faults (Chen, 1992). Correlating the data with mantle-derived helium, samples WX3, 6, and 10 in Figure 4 exhibit relatively high $\delta^{13}\text{C}_{\text{CO}_2}$ values but do not have correspondingly high mantle-derived helium or CO_2 content. However, according to Table 2, samples 6 and 10 have high radon values, and sample 6 shows frequent values exceeding 2,000 Bq/L, indicating the presence of higher U and Th content in the deep rocks. It is inferred that the contribution rate of mantle-derived $\delta^{13}\text{C}_{\text{CO}_2}$ is higher at these three sampling points. The presence of higher crustal-derived ^4He results in distorted mantle-derived helium values. Based on Figure 3, samples 2, 4, 8, 9, 20, 22, and 29 have higher contributions from organic sources compared to other sampling points. This observation aligns with the fact that these gas samples were taken from bathing pools or fields, where the water temperature is relatively low. Sample 21 is special. It is a cold spring with a water temperature of only 19.1°C , located beside a small stream. However, its contribution from organic



sources is not particularly high, and it has higher $\delta^{13}\text{C}_{\text{CO}_2}$ values and significantly elevated R values, suggesting the presence of gases from deep sources despite being a cold spring. As a result, it exhibits excellent responsiveness to global and regional seismic events, such as the 2004 Indonesia $M_s 8.7$ earthquake, the 2011 Japan $M_s 9.0$ earthquake, the 1976 Tangshan $M_s 7.6$ earthquake, and the 2008 Wenchuan $M_s 8.0$ earthquake, where the water turned turbid and continued for several days.

5.2 Heat flow and lithospheric thermal structure

Geothermal heat flux (q , mW/m^2) is the most direct manifestation of the Earth's internal heat at the surface. It comprises two components: heat from the deep Earth and heat generated by the decay of radioactive elements in the Earth's crust and rocks, namely, mantle heat flow (q_m) and crustal heat flow (q_c). It provides insights into the activity of the Earth's crust and upper mantle in the region. Since the production of ^3He from radiogenic processes can be considered negligible compared to the escape of ^3He from the mantle, the ^3He content is directly proportional to the mantle heat flux, while the ^4He content is linearly correlated with the crustal heat flux. The following equations can be utilized to estimate q_m , q_c , and the percentage of mantle-derived heat flow (%) (Polyak et al., 1979; O'Nions and Oxburgh, 1983; O'Nions and Oxburgh, 1988; Wang, 1999):

$$q = 18.231 \log R_c + 181.82 \quad (1)$$

$$\frac{q_c}{q_m} = 0.815 - 0.3 \ln R \quad (2)$$

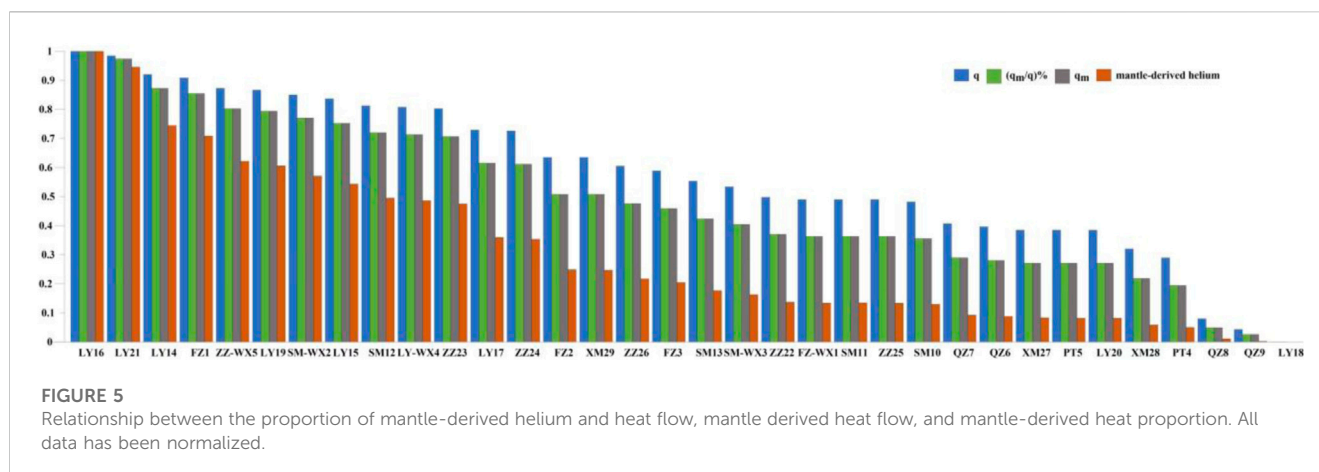
where R is the He isotopic ratios, R_c is the corrected He isotopic ratios, q (mW/m^2) is the Geothermal heat flux, q_c (mW/m^2) is the crustal heatflow, and q_m (mW/m^2) is the mantle heatflow.

The calculated results are shown in Table 2. The geothermal heat flux values reflect the thermal background of the Fujian region, ranging from 53 to 81 mW/m^2 , with an average of 69 mW/m^2 , which is higher than the average heat flux value of 63 mW/m^2 for Chinese

mainland (Hu et al., 2000), and is consistent with the average heat flux value in the South China region. Spatially, the western part of Fujian has higher heat flux values, particularly in the Longyan area, such as points 14, 15, 16, 19, and 21, with point 16 having the highest heat flux value in the entire province. The southeastern coastal area of Minnan, including points 4, 5, 27, and 28, has lower heat flux values. These results are generally in agreement with previous studies on heat flow data (Wang and Huang, 1988; Wang and Huang, 1990; Xiong et al., 1992; Hu, 1992; Hu and Wang, 1994; Hu et al., 2000; Hu et al., 2001; Jiang et al., 2016; Jiang et al., 2019). The average heat flux value of the six measurement points in Zhangzhou is 72 mW/m^2 , which is quite consistent with the mean value of 73 mW/m^2 obtained by previous studies through comprehensive calculations using geothermal, geochemical, and hydrogeological data (Zhuang, 2010).

In the study area, the crustal heat flux values show little variation, ranging from 30 to 35 mW/m^2 , with a maximum difference of only 5 mW/m^2 . In contrast, the mantle heat flux values exhibit a larger range, varying from 20 to 52 mW/m^2 , with a maximum difference of 32 mW/m^2 . This indicates that the variation in geothermal heat flux values in Fujian is mainly attributed to the contribution of mantle-derived heat. As shown in Figure 5, the geothermal heat flux value, mantle heat flux value, and percentage of mantle-derived heat are positively correlated with the percentage of mantle-derived helium, indicating that the percentage of mantle-derived helium is a good indicator for identifying areas with thermal anomalies. According to Table 2, the percentage of mantle-derived heat ranges from 38% to 63%, with a maximum difference of 25%. Among all measurement points, 44% have a mantle-derived heat contribution of over 50%, suggesting that mantle heat flux is a significant source of heat in the Fujian region. This is a key factor contributing to the higher geothermal heat flux values in Fujian compared to the average value for Chinese mainland.

Regarding the distribution of hot springs, they mainly occur along NE and NW trends in a bead-like pattern. More hot springs with higher water temperatures are distributed along NE direction (as shown in Figure 1A; all six hot springs with temperatures above



80°C are distributed along the NE direction), while the temperatures of NW-direction hot springs are mostly below 70°C or lower, indicating that the distribution of geothermal anomalies is strongly influenced by NE-trending deep-seated faults. Meanwhile, as shown in Figure 1B, seismic records of earthquakes with magnitudes greater than 5 and various periods of granite intrusions (Figure 1D) are also distributed along the NE direction, suggesting that the heat source of underground hot water is primarily controlled by NE-trending structures. Hot springs are most concentrated around the F2 region and its vicinity, which is the center of Mesozoic magmatism, with the most intense intrusive activity (Wang et al., 1993). This indicates that the occurrence of hot springs is closely related to magma intrusive activities and deep-seated faults in the F2 region.

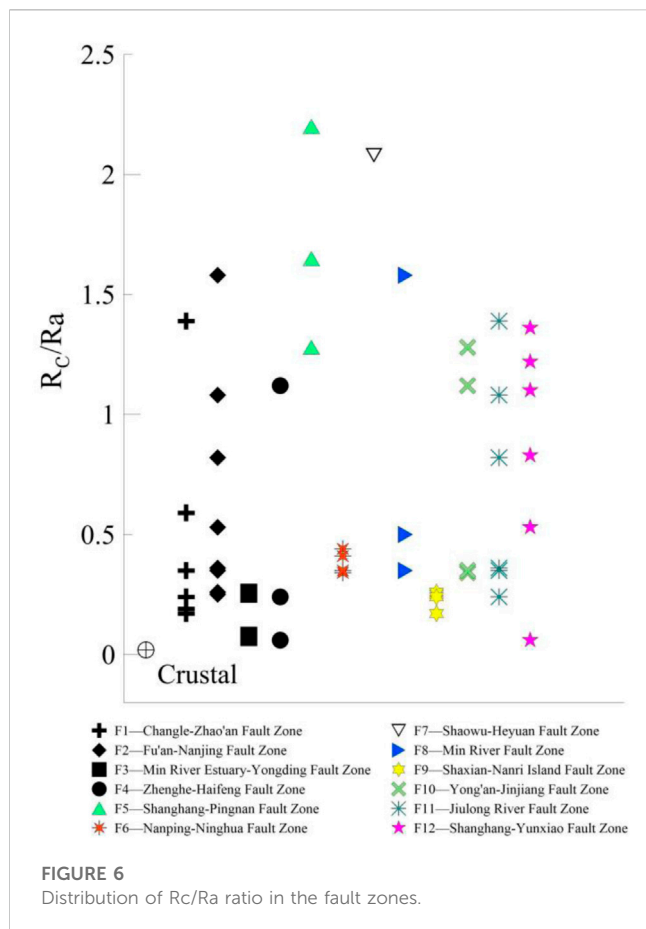
The NW structural zone in the research area represents the most recent tectonic activity, largely intersecting with other structural trends. Its mechanical properties mainly involve shear, tensional, and transtensional fault zones exhibiting high dip angles of 60° or more, particularly pronounced in F8 and F11 with dip angles reaching 75°–85°. The area demonstrates relatively good connectivity and aquifer properties for groundwater, serving as the primary supply source for underground hot springs and advantageous pathways for spring upwellings. The intersecting patterns of NW-oriented F8 and F11 with NE-oriented F4, F2, F1, and their intersection area form a checkerboard-like structure that facilitates the ascent of mantle-derived heat, with F11 cutting through the urban area of Zhangzhou at the steepest angle, interacting with F2. Consequently, Zhangzhou stands out as the region with the highest density and highest water temperature of hot springs within the study area, with its R/Ra values ranking among the highest in the province. In summary, the heat sources of all these hot springs are primarily from mantle heat superimposed by the radiogenic heat-producing elements from the late Mesozoic granites. All these hot springs distributed along NE and NW oriented fault zones primarily associated with vertical tectonic movements during the Cenozoic (Zhang et al., 2018). Stress-weakened zones, such as the edges of plutonic intrusion, late-stage dykes, or contact zones between intrusive bodies and strata, are commonly observed locations of hot springs exposure, such as SM10, LY16, SM12, and LY14. All these observations align with

previous reports of hot springs in the Guangdong and Tan-Lu fault zones region (Wang, 2018).

5.3 Indications of the geochemically spatial distribution of hot spring gas on the tectonic environment of Fujian Province

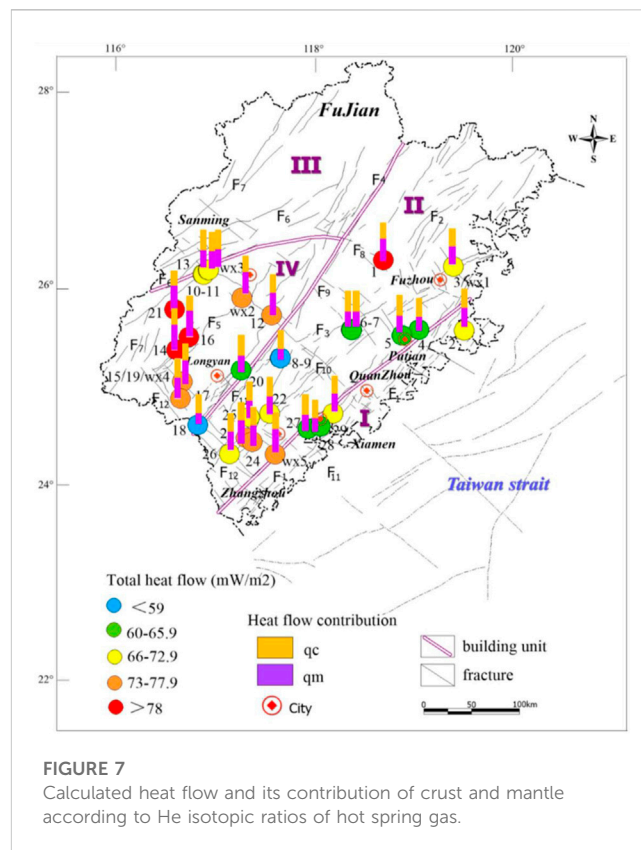
Based on the previous discussion, it can be inferred that the deep-large fault controls the magma intrusion, convection, and occurrence, exposure, and distribution of hot springs in the Fujian region, serving as a crucial conduit for deep mantle-derived heat flow and with R/Ra providing significant thermal anomaly indicators. In fact, previous researchers have noted a good correlation between the distribution of $^3\text{He}/^4\text{He}$ values and the regional tectonic environment in China. High $^3\text{He}/^4\text{He}$ values are associated with intense tectonic activity, while low values indicate a more stable tectonic setting (Xu et al., 1997). Mantle convection heat also influences and governs variations in the lithospheric mantle thickness (Zhao et al., 1995). Therefore, the spatial distribution characteristics of R/Ra can be used to reveal and explore the deep and shallow tectonic environments and the degree of crust-mantle connection in the region. Fujian, situated at the forefront of the South China continental margin, has radiogenic heat from shallow crustal granites as a significant heat source for hydrothermal activity. However, calculations from Table 2 indicate that mantle convection heat contributes to an average of 50%, with a minimum of 38%. Thus, Fujian holds importance as a research site for studying crust-upper mantle structure and geothermal activities. However, the current studies on deep structural environments in Fujian from a geochemical perspective are rare. Previous studies mainly employed geophysical exploration methods such as controlled source seismicity, microseismicity, magnetotelluric sounding, heat flow measurements, paleomagnetic analyses, and remote sensing (Chen, 1992; Wang et al., 1993; Ma, 2002; Cai et al., 2016; Teng et al., 2019).

From Figure 6, it can be observed that the high R/Ra values above 1.5 are located along the NE-trending fault, indicating that the NE-trending fault has a larger scale and deeper cutting compared to the NW-trending fault. However, both NE- and NW-trending faults show scattered R/Ra values with high, medium, and low values,



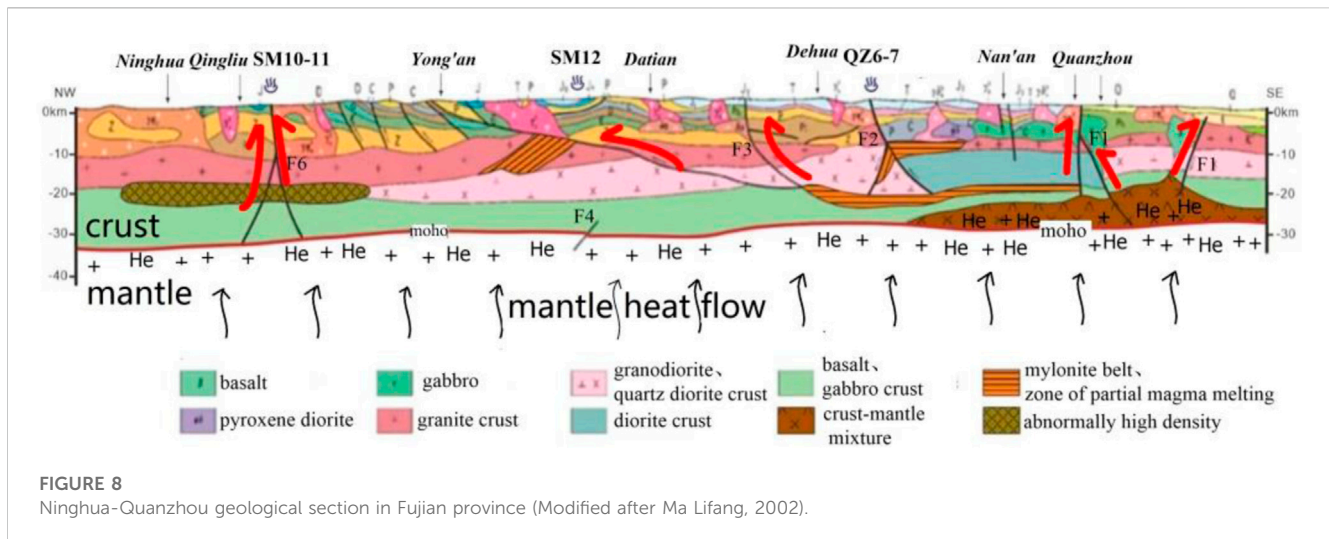
suggesting variations in cutting depth along the same fault zone in different areas. From the perspective of mantle convection heat influence and the variation of lithospheric mantle thickness, it is inferred that the crustal thickness in both NE and NW directions is uneven, with fluctuations in the Moho interface. Particularly, F1 and F2 are located at the forefront of the Fujian continental margin, where the R_c/R_a values show the highest fluctuations. It is speculated that the Moho interface in the southeast coastal area of Fujian is undulated. As seen in Figures 1A,B, the region between F1 and F2 in the eastern part is dense in hot springs and seismic activities, with the highest distribution of hot springs above 70°C. This is attributed to the intense neotectonic activity during the Late Yanshanian and Early Himalayan periods, with Fujian being in a landward extensional environment, characterized by mantle-derived underplating and lithospheric thinning (Li et al., 2018; 2019). The deep intrusion of these underplating fluids along fault channels is the dynamic factor responsible for the uneven crustal thickness and undulations.

It is worth noting that several measurement points at the intersections of the NE and NW fault zones, such as FZ1 (the intersection of F2 and F8), WX2 (the intersection of F5 and F10), and SM12 (the intersection of F4 and F10), exhibit significantly higher R_c/R_a and mantle thermal convection values compared to the surrounding points (Figure 7; Table 2), with mantle-derived heat proportions exceeding 50%, reaching 60%, 57%, and 56%, respectively. The strong mantle convection heat in these areas suggests that the fault intersection zones serve as favorable



pathways for mantle-derived heat material upwelling. It is inferred that these fault zones cut exceptionally deep at their intersections, constituting ultra-crustal faults. Moreover, the high mantle heat proportions also suggest a high degree of crust-mantle connectivity, indicating the possible existence of mantle underplating at depth. This inference is consistent with the geological cross-section of Ninghua-Quanzhou in Fujian Province (Figure 8), which shows that the NE-trending fault has a larger scale and deeper cutting, with the F6 on the west and F1 on the east being ultra-crustal faults that cut through the Moho interface, and the F4 in the middle showing obvious Moho discontinuity. This is also in line with the findings of Liao et al. (1990) that there is a clear discontinuity in the upper mantle beneath Fuzhou Basin, with a displacement of 3 km, and the presence of mantle-derived deep-seated xenoliths (pyrope peridotite) in the ~136 km mantle-derived olivine basalts exposed in the FZ1 area (Liu et al., 1985).

It is worth mentioning that QZ6-7 and SM10-11, located at the intersections of the NE and NW fault zones, did not exhibit high R_c/R_a values. This is because they are situated in high U and Th rock areas, but their corresponding $\delta^{13}C_{CO_2}$ values indicate a deep-source signal, as mentioned previously. In Figure 8, it can be observed that F2 in the area of Dehua cuts into the lower crust, and QZ6-7 has two layers of upwelling magma-melting zones of upper mantle in the middle and lower crust. The high conductivity geological body peak values are located at 10 km and 20 km depths (Wang et al., 1993), and they are connected with the fault structures, providing a heat source and deep-seated fluids for QZ6-7. The research on the crustal and upper mantle velocity structure in Fujian also suggests the existence of uplift in the lower crust in the Nancheng hot spring area



(Cai et al., 2016). Due to this deep heat source, the Nancheng hot spring in Dehua has become the hottest spring in eastern China. Figure 8 also shows that an abnormally high-density body appears in the lower crust of the Qingliu area where SM10-11 is located, and the underlying F6 cuts into the Moho interface. Field investigations have also discovered ultrabasic rock occurrences, all of which indicate a high degree of crust-mantle connectivity in this region.

In summary, Rc/Ra has indicative significance for deep structural environments. Locations with high Rc/Ra and a high proportion of mantle-derived heat usually have a high degree of crust-mantle connectivity. The fault zones in such areas generally exhibit deep cutting and large scales, often being ultra-crustal faults. The presence of high-conductivity or low-velocity layers such as magmatic melts in the lower crust indicates the tectonic environments such as upwelling mantle diapir, mantle doming, and crustal thinning. If basaltic rocks are exposed around it, it is likely to reveal the existence of Moho subsidence and Moho discontinuity.

5.4 Hot spring gas and seismic activity

Research on the spatio-temporal characteristics of seismic activity and its correlation with hot springs in the study area reveals a consistent distribution pattern between seismicity and hot spring occurrence. The northeastern part of Fujian province, where hot springs are scarce, experiences minimal seismicity, whereas seismic events predominantly occur in the hot spring-dense regions of northwestern and southern Fujian. Furthermore, regions with stronger mantle convection heat exhibit higher seismic frequency and intensity (Figure 1B; Figure 7). Longyan region stands out as the area with the highest Rc/Ra values in the entire province, with a mantle-derived heat proportion reaching 63%, signifying the most vigorous mantle-derived heat flow in the province. Figure 1B shows that the area near by F5 has a history of experiencing significant seismic events. Since 1971, two of the three $M_L 5.0$ or above earthquakes in Fujian's continental area have occurred in this vicinity. It is speculated that these seismic events are closely related to intense mantle convection heat, and deep-seated heat fluid

upwelling is the primary driving force behind the seismic anomalies in this region. As the mantle material ascends, it destabilizes the crust, and the disruption of dynamic equilibrium in mantle thermal convection leads to the accumulation of thermal energy in confined spaces, creating a potential force. Once this force reaches its limit, it releases the accumulated heat into the atmosphere, resulting in seismic vibrations—what we commonly observe as moderate to small earthquakes. In essence, these moderate to small earthquakes also function as a means for the Earth to regulate the thermal energy balance between the geosphere and the atmosphere.

5.5 Hot spring outgassing and seismic activity in Taiwan

The process of seismic birth and development is always accompanied by the movement of subsurface materials, energy transfer, and changes in conditions, leading to the migration and evolution of elements and isotopes in fluids, thereby forming observable fluid geochemical anomalies on the Earth's surface (Li, et al., 2022). Geoscientists have been exploring effective short-term precursors of earthquakes and have made some significant progress over the years, with geochemical components being particularly prominent in this regard. Both ions and gases have yielded some seismic examples (Chen et al., 2014; Marin, et al., 2010; Wang, et al., 1991; Zhang, et al., 1993; Liao, et al., 2010; Liao, et al., 2022).

A correlation analysis between the observation results and earthquakes of $M_L 6$ or higher in Taiwan during the same period (Table 3). Spatial distribution of earthquakes can be seen in Figure 1C. From Figure 9, it is evident that since the initial observation of QZ6 gas flow velocity, it has consistently fluctuated around the mean line (represented by the middle dashed line). The upper (value=0.548 mL/s) and lower (value=0.173 mL/s) dashed lines represent empirical threshold lines summarized in July 2022. Almost all strong earthquakes of $M_L 6$ in Taiwan exhibited precursor anomalies, except for the $M_L 6.0$ earthquake in the Hualien Sea area which occurred 1 day after

TABLE 3 M_L 6.0 or above earthquakes that have occurred in Taiwan since 2021 (Data of earthquakes are from Taiwan's Central Meteorological Bureau).

No	Origin time	Location	$\lambda E(^{\circ})$ $\phi N(^{\circ})$	magnitude (M_L)	Source depth (km)
1	2021-4-18	HuaLian	121.48,23.86	6.2	14.4
2	2021-8-5	HuaLian Sea	122.32,24.80	6.0	7.0
3	2021-10-24	YiLan	121.78,24.53	6.5	65.6
4	2022-1-3	HuaLian Sea	122.17,24.02	6.0	22.4
5	2022-3-23	TaiDong Sea	121.61,23.40	6.7	25.7
6	2022-5-9	HuaLian Sea	122.53,23.97	6.2	16.8
7	2022-6-20	HuaLian	121.45,23.69	6.0	7.0
8	2022-9-17	TaiDong	121.16,23.08	6.6	8.6
9	2022-9-18	HuaLian	121.20,23.14	6.8	7.8
10	2022-12-15	HuaLian Sea	121.85,23.78	6.4	16.3

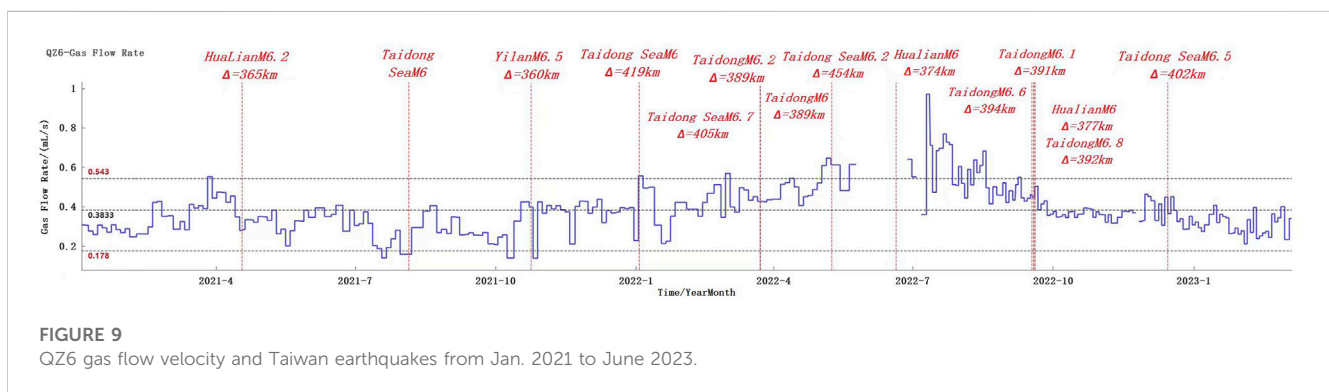


FIGURE 9 QZ6 gas flow velocity and Taiwan earthquakes from Jan. 2021 to June 2023.

crossing the empirical threshold. For instance, events numbered eight to nine occurred 2 months before, crossing the super-empirical threshold, with an abnormal duration of 1 month. This event was, in fact, the most intense seismic activity observed in Taiwan since the start of the observations, forming an earthquake cluster. According to data from the Central Weather Bureau in Taiwan, only from September 17 to 19, 2022, eight earthquakes with magnitudes ranging from M_L 5.0 to 5.9 and two earthquakes with magnitudes between M_L 6.0 and 6.9 were recorded. The other six earthquakes occurred three to 21 days before crossing the super-empirical threshold. QZ6 gas flow velocity exhibits a good short-term predictive indicator.

The quarterly tests of helium and carbon isotopes in the outflow gas of hot springs have also captured multiple observations of enhanced deep-seated information in several hot springs before several M_L 6 earthquakes in Taiwan. The highest R/Ra values of FZ1, LY14, LY16, and SM12 all occurred around 10 days before the occurrence of M_L 6 earthquakes in Taiwan. The highest $\delta^{13}C_{CO_2}$ values observed for SM12 and FZ1 also appeared within 10 days before M_L 6 earthquakes in Taiwan (Figure 10; Table 4). Similar isotopic value increases in hot spring gases were also observed before and after the 2008 Wenchuan M_s 8.0 earthquake and the 2016 Litang M_s 5.1 earthquake (Zhou et al., 2015; Zhou et al., 2017).

These observations indicate a rough correlation between the observed gas anomalies in Fujian's hot springs and M_L 6 earthquakes in Taiwan. Previous studies analyzing seismic source mechanisms in

the Fujian region have revealed that the stress field's P-axis direction is NW-SE, and the main driving force for tectonic stress comes from the dynamic force from the Taiwan Strait to the mainland (Shi et al., 2006). It is inferred that this force originates from the impact of the Philippine Sea Plate's subduction and thrusting on the eastern side of Taiwan. Taking the 2022 Hualien M_L 6.8 earthquake in Taiwan as an example, the main fault for this earthquake is the Chihshang-Yuli active fault within the Hualien Longitudinal Valley fault zone, with the driving force coming from the northwestward thrust of the Philippine Sea Plate. QZ6 and SM12 are located on the stress axis of the Philippine Sea Plate thrusting towards the Eurasian Plate, experiencing stress transmission due to the compressional forces from the plate. The gas flow velocity and isotopic content of hot spring gases will increase with the increasing crustal stress. Figure 11 illustrates this stress transmission mode between the Fujian and Taiwan plates.

6 Conclusion

- (1) The dominant constituents of the escaping gas from the hot springs in the research area are nitrogen (N_2), and the helium content in the hot spring gases primarily originates from the Earth's crust. Hot springs exhibiting elevated $^3He/^4He$ ratios imply a significant proportion of mantle-derived helium. Moreover, the low concentration of carbon dioxide (CO_2)



TABLE 4 $\delta^{13}\text{C}_{\text{CO}_2}$ seismic reflection of typical hot spring gases in Fujian.

Sampling site	SM12						FZ1			
	2021/5/25	2021/9/10	2021/12/28	2022/3/10	2022/7/4	2022/9/22	2021/4/13	2021/9/11	2022/1/22	2022/9/23
$\delta^{13}\text{C}_{\text{CO}_2}$	-13.5	-13.9	-11.5	-14.4	-14.3	-13.6	-12.5	-13.5	-13.4	-12.5
Note	—	—	6 days before the earthquake	—	—	—	5 days before the earthquake	—	—	5 days after the earthquake

Times are highlighted in bold.

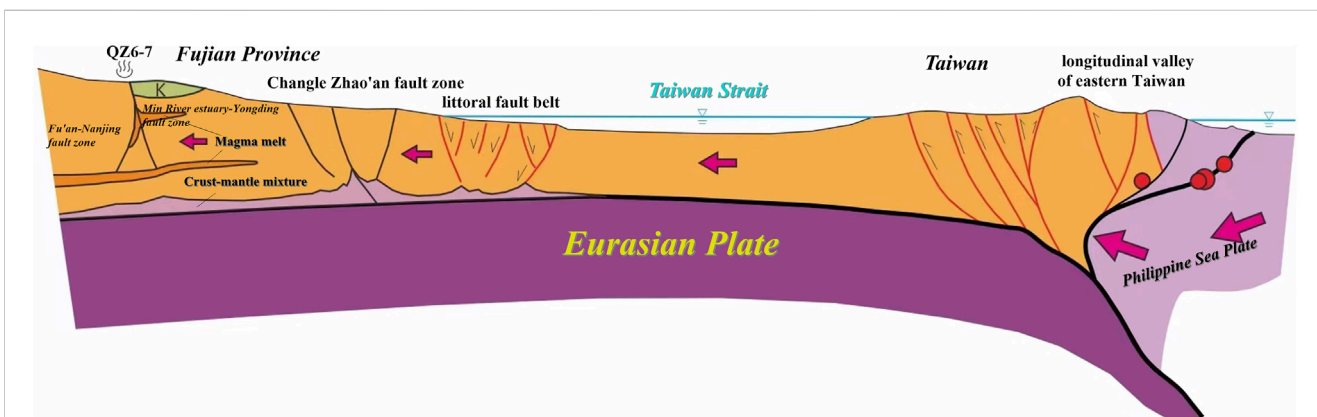


FIGURE 11 Schematic cartoon showing the stress transmission mode between the Fujian and Taiwan plates.

and elevated $\delta^{13}\text{C}_{\text{CO}_2}$ and $^3\text{He}/^4\text{He}$ values in the hot spring gases suggest contributions from deep-seated CO_2 sources. However, it is essential to acknowledge that high uranium (U) and thorium (Th) contents in the rocks can lead to enhanced α -decay-produced ^4He , potentially distorting the $^3\text{He}/^4\text{He}$ ratios and consequently not unequivocally aligning with elevated $^3\text{He}/^4\text{He}$

values. In such cases, the inclusion of radon (gas) emissions can serve as a complementary means for precise evaluations. (2) The variations in helium isotopic ratios ($^3\text{He}/^4\text{He}$) of the hot spring gases in the research area span between 0.06 and 2.41Ra. The computation of $^3\text{He}/^4\text{He}$ ratios indicates a maximum proportion of mantle-derived helium, reaching 30.19%. This

signifies considerable mantle degassing, indicative of deep-seated structures, such as fault-connected mantle or mantle doming. These hot springs manifest a pronounced association with the NE-oriented fault zone in the region and historical earthquakes of M_s 5 or above. Notably, regions characterized by intensified mantle thermal convection exhibit augmented earthquake frequency and intensity, while areas with scarce hot spring occurrences tend to minimal seismic activity. Consequently, deep-seated thermal fluid upwelling within the Earth's interior emerges as the impelling mechanism behind seismic activity within these geothermal anomaly regions.

- (3) The thermal flow values in the crustal domain within the research area exhibit limited variability. The magnitudes of crustal heat flow, mantle heat flow, and the proportion of mantle-derived heat display a positive correlation with mantle-derived helium. Noteworthy distinctions in crustal heat flow values predominantly emanate from contributions attributable to mantle-derived heat. The deduced proportion of mantle-derived heat ranges between 37.61% and 63.35%, with the highest value attaining 63.35%. This conspicuous prevalence of mantle-derived heat stands as the primary factor underpinning the elevation of heat flow values within the research area, surpassing the national average heat flow values of mainland China.
- (4) The results of the correlation analysis on seismic activity of magnitude 6 in Taiwan show that high values of hot spring gas flow velocity, $^3\text{He}/^4\text{He}$, and $\delta^{13}\text{C}_{\text{CO}_2}$ in the time domain provide significant short-term anomalous indications for M_L 6 earthquakes in the Taiwan region. Consequently, employing gas flow rate and helium-neon-carbon isotope observations in natural hot springs within the research area holds paramount significance in facilitating short-term and imminent analyses of M_L 6.0 and above earthquakes in Taiwan.

Data availability statement

The original contributions presented in the study are included in the article/Supplementary Material, further inquiries can be directed to the corresponding authors.

References

- Arnorsson, S. (2000). *Isotopic and chemical techniques in geothermal exploration, development and use*. Vienna, Austria: International Atomic Energy Agency.
- Cai, H. T., Jin, X., Wang, S. X., et al. (2016). The crust structure and velocity structure characteristics beneath Ninghua-Datian-Hui'an. *Chin. J. Geophys.* 59 (1), 157–168. doi:10.6038/cjg20160113
- Chen, Z., Du, J., Zhou, X., Yi, L., Liu, L., Xie, C., et al. (2014). Hydrochemistry of the hot springs in western sichuan province related to the wenchuan ms 8.0 earthquake. *Sci. World J.* 2014, 1–13. doi:10.1155/2014/901432
- Chen, Z., Zhou, X., Du, J., Xie, C., Liu, L., Li, Y., et al. (2015). Hydrochemical characteristics of hot spring waters in the Kangding district related to the Lushan $M=7.0$ earthquake in Sichuan, China. *Nat. Hazards Earth Syst. Sci.* 15, 1149–1156. doi:10.5194/nhess-15-1149-2015
- Chen, Z. J. (1992). *Research on geothermal geophysics in Fujian province*. Beijing, China: Science and Technology of China press.
- Cheng, Y., Han, B., Li, Y., Guo, J., and Hu, X. (2021). Lithospheric electrical structure beneath the cathaysia block in South China and its tectonic implications. *Tectonophysics* 814, 228981. doi:10.1016/j.tecto.2021.228981
- Craig, H., Lupton, J. E., Welhan, J. A., and Poreda, R. (1978). Helium isotope ratios in yellowstone and lassen park volcanic gases. *Geophys. Res. Lett.* 5 (11), 897–900. doi:10.1029/GL005i011p00897
- Dai, Jinxing, Ni, Yunyan, Liu, Quanyou, Wu, Xiaqi, Yu, Cong, Gong, Deyu, et al. (2022). Carbon dioxide and its carbon isotopic composition of natural gas in the Sichuan Basin, SW China. *Front. Earth Sci.* 10, 857876. doi:10.3389/feart.2022.857876
- Dai, J. X. (1993). Characteristics of hydrocarbon isotopes in natural gas and identification of various types of natural gas. *Nat. Gas. Geosci.* 10 (2), 1–40.
- Du, J. G., Wang, X. B., and Xie, H. S. (1994). Mantle degassing-A Gasgeochemical feature of deep Earth Matter movement. *Adv. Earth Sci. Chin.* 9 (3), 48–52.
- Duchkov, A. D., Rychkova, K. M., Lebedev, V. I., Kamenskii, I. L., and Sokolova, L. S. (2010). Estimation of heat flow in Tuva from data on helium isotopes in thermal mineral springs. *Russ. Geol. Geophys.* 51 (2), 209–219. doi:10.1016/j.rgg.2009.12.023

Author contributions

LL: Writing–original draft. YZ: Writing–review & editing. ZL: Writing–review & editing. XW: Writing–review & editing. WC: Writing–review & editing. JiyL: Writing–review & editing. CZ: Writing–review & editing. WY: Writing–review & editing. XL: Writing–review & editing. JiaL: Writing–original draft.

Funding

The author(s) declare financial support was received for the research, authorship, and/or publication of this article. This study was financially supported by Earthquake Science and Technology Spark Program Research Project of China Earthquake Administration (No. XH21013) and the National Key Research and Development Program of China (No.: 2019YFC1509404).

Acknowledgments

We thank Profs. Zhang Zhaochong, JL Yaowei and YZ Xiaocheng for their constructive comments. Profs. Li Liwu and Xing Lantian are appreciated for their support in observing helium neon carbon isotopes and hot spring gas volume percentages.

Conflict of interest

The authors declare that the research was conducted in the absence of any commercial or financial relationships that could be construed as a potential conflict of interest.

Publisher's note

All claims expressed in this article are solely those of the authors and do not necessarily represent those of their affiliated organizations, or those of the publisher, the editors and the reviewers. Any product that may be evaluated in this article, or claim that may be made by its manufacturer, is not guaranteed or endorsed by the publisher.

- Fridriksson, T., Padrón, E., Óskarsson, F., and Pérez, N. (2016). Application of diffuse gas flux measurements and soil gas analysis to geothermal exploration and environmental monitoring: example from the reykjanes geothermal field, sw Iceland. *Renew. Energy* 86, 1295–1307. doi:10.1016/j.renene.2015.09.034
- Geology investigation institute of Fujian province, (2016). *Regional geology of fujian*. Beijing, China: Geological publishing house.
- Giggenbach, W. F., Tedesco, D., Sulistiyo, Y., Caprai, A., Cioni, R., Favara, R., et al. (2001). Evaluation of results from the fourth and fifth IAVCEI field workshops on volcanic gases, Vulcano island, Italy and Java, Indonesia. *J. Volcanol. Geotherm. Res.* 108 (1), 157–172. doi:10.1016/s0377-0273(00)00283-3
- Guo, Q. H. (2022). Magmatic heat source geothermal system and its hydrogeochemical criteria. *J. Geol.* 96 (1), 208–214. doi:10.19762/j.cnki.dizhixuebao.2022035
- He, Y. J., and Chen, M. G. (1999). Characters and thermal source of hot springs in fujian province. *Geol. Fujian* 18 (3), 149–155.
- Hu, S. B., He, L. J., and Wang, J. Y. (2001). Compilation of heatflow data in the Chinese mainland area (3rd Edition). *Chinese Journal Geophys.* 44 (5), 611–626.
- Hu, S. B. (1992). Research progress on the relationship between vertical distribution of crustal radioactive heat production rate and seismic wave velocity structure. *Foreign Geol. (Beijing)* 2, 1–8.
- Hu, S. B., and Wang, J. Y. (1994). Crustal heat generation rate and mantle heat flow in southeast China. *Sci. China (Series B)* 24 (2), 185–193.
- Hu, S., He, L., and Wang, J. (2000). Heat flow in the continental area of China: A new data set. *Earth Planet. Sci. Lett.* 179 (2), 407–419. doi:10.1016/s0012821x(00)00126-6
- Italiano, F., Bonfanti, P., Pizzino, L., and Quattrocchi, F. (2010). Geochemistry of fluids discharged over the seismic area of the southern apennines (calabria region, Southern Italy): implications for fluid–fault relationships. *Appl. Geochem.* 25 (4), 540–554. doi:10.1016/j.apgeochem.2010.01.011
- Javoy, M., Pineau, F., and Delorme, H. (1986). Carbon and nitrogen isotopes in the mantle. *Chem. Geol.* 57 (1–2), 41–62. doi:10.1016/0009-2541(86)90093-8
- Jiang, G., Hu, S., Shi, Y., Zhang, C., Wang, Z., and Hu, D. (2019). Terrestrial heat flow of continental China: updated dataset and tectonic implications. *Tectonophysics* 753, 36–48. doi:10.1016/j.tecto.2019.01.006
- Jiang, G. Z., Gao, P., Rao, S., Zhang, L. Y., Tang, X. Y., Zhao, P., et al. (2016). Compilation of heatflow data in the continental area of China. *Chin. J. Geophys.* 59 (8), 2892–2910. doi:10.6038/cjg20160815
- Li, J., Pang, Z. H., Yang, G. M., Tian, J., Tong, A. L., Zhang, X. Y., et al. (2017). Million-year-old groundwater revealed by krypton-81 dating in Guanzhong Basin, China. *Sci. Bulletin* 62 (17), 1181–1184. doi:10.1016/j.scib.2017.08.009
- Li, S. Z., Cao, X. Z., Wang, G. Z., et al. (2019). Meso-cenozoic tectonic evolution and plate reconstruction of the Pacific plate. *J. Geomechanics* 25 (5), 642–677. doi:10.12090/j.issn.1006-6616.2019.25.05.060
- Li, S. Z., Suo, Y. H., Li, X. Y., Wang, Y., Cao, X., Wang, P., et al. (2018). Mesozoic plate subduction in West Pacific and tectono-magmatic response in the East Asian ocean-continent connection zone. *Chin. Sci. Bull.* 63 (16), 1550–1593. doi:10.1360/n972017-01113
- Li, Y., Chen, Z., Hu, L., Su, S., Zheng, C., Liu, Z., et al. (2022). Advances in seismic fluid geochemistry and its application in earthquake forecasting. *Chin. Sci. Bull.* 67, 1404–1420. doi:10.1360/tb-2021-0955
- Liao, L. X., et al. (2010). Analysis on the difference of reflecting characteristics of hydro-radon in Huanan-Tainei well to earthquakes in Fujian and Taiwan region. *Earthquake* 30 (4), 133–139.
- Liao, L. X., Qin, S. L., and Mo, P. C. (2022). Extraction and application of fluid prediction index in South China. *South China J. Seismol.* 42 (4), 67–77. doi:10.13512/j.hndz.2022.04.10
- Liao, Q. L., Wang, Z. M., Qiu, T. X., Yuan, D. Q., Wang, H. T., Wu, N. Y., et al. (1990). Study on the deep crustal structure and tectonics of the Fuzhou Basin and its surrounding Areas. *Chin. J. Geophys.* 33 (2), 163–173.
- Liu, Quanyou, Wu, Xiaoqi, Jia, Huichong, Ni, Chunhua, Zhu, Jianhui, Miao, Jiujun, et al. (2022). Geochemical characteristics of helium in natural gas from the Daniudi gas field, Ordos Basin, central China. *Front. Earth Sci.* 10, 823308. doi:10.3389/feart.2022.823308
- Liu, Quanyou, Jin, Zhijun, Wu, Xiaoqi, Liu, Wenhui, Gao, Bo, Zhang, Dianwei, et al. (2014). Origin and carbon isotope fractionation of CO₂ in marine sour gas reservoirs in the Eastern Sichuan Basin. *Org. Geochem.* 74, 22–32. doi:10.1016/j.orggeochem.2014.01.012
- Liu, Quanyou, Wu, Xiaoqi, Wang, Xiaofeng, Jin, Zhijun, Zhu, Dongya, Meng, Qingqiang, et al. (2019). Carbon and hydrogen isotopes of methane, ethane, and propane: A review of genetic identification of natural gas. *Earth-Science Rev.* 190, 247–272. doi:10.1016/j.earscirev.2018.11.017
- Liu, R. X., Fan, Q. C., and Sun, J. Z. (1985). Study on garnet lherzolite xenoliths from eastern China. *Acta Petrol. Sin.* 1 (4), 24–33.
- Lowenstern, Jacob B., Bergfeld, Deborah, Evans, William C., and Hunt, Andrew G. (2015). Origins of geothermal gases at Yellowstone. *J. Volcanol. Geotherm. Res.* 302, 87–101. doi:10.1016/j.jvolgeores.2015.06.010
- Ma, L. F. (2002). *Geological atlas of China*. Beijing, China: Geological publishing house.
- Marco, T., Barbara, N., Orlando, V., Santiago, M., Diego, M., and Alberto, R. (2021). Soil CO₂ flux and temperature from a new geothermal area in the Cordón de Inacaliri Volcanic Complex (northern Chile). *Geothermics* 89, 101961. doi:10.1016/j.geothermics.2020.101961
- Marin, C., Mitrofan, H., Dinu, I., et al. (2010). Deciphering hydrochemical information provided by saline springs in the Carpathians bend area: a strong Vrancea earthquake expected to occur earlier than 2012. *Geocomarina*. doi:10.5281/ZENODO.56963
- O’Nions, R. K., and Oxburgh, E. R. (1983). Heat and helium in the Earth. *Nature* 306 (5942), 429–431. doi:10.1038/306429a0
- O’Nions, R. K., and Oxburgh, E. R. (1988). Helium, volatile fluxes and the development of continental crust. *Earth Planet. Sci. Lett.* 90 (3), 331–347. doi:10.1016/0012-821X(88)90134-3
- Peng, Weilong, Liu, Quanyou, Zhang, Ying, Jia, Huichong, Zhu, Dongya, Meng, Qingqiang, et al. (2022). The first extra-large helium-rich gas field identified in a tight sandstone of the Dongsheng Gas Field, Ordos Basin, China. *Sci. China Earth Sci.* 65 (5), 874–881. doi:10.1007/s11430-021-9898-y
- Pinti, D. L., Castro, M. C., Shouakar Stash, O., Tremblay, A., Garduno, V. H., Hall, C. M., et al. (2013). Evolution of the geothermal fluids at Los Azufres, Mexico, as traced by noble gas isotopes, $\delta^{18}\text{O}$, δD , $\delta^{13}\text{C}$ and $87\text{Sr}/86\text{Sr}$. *J. Volcanol. Geotherm. Res.* 249, 1–11. doi:10.1016/j.jvolgeores.2012.09.006
- Polyak, B. G., Tolstikhin, I. N., and Yakutse, V. P. (1979). The isotopic composition of helium and heat–flow–geochemical and geophysical aspects of tectogenesis. *Geotectonics* 13 (5), 339–351.
- Sano, Y., and Marty, B. (1995). Origin of carbon in fumarolic gas from island arcs. *Chem. Geol.* 119 (1), 265–274. doi:10.1016/0009-2541(94)00097-r
- Shi, L. H., Zhou, Z. R., Bao, T., and Ni, X. Y. (2006). Discussion of force source of seismic activity in Fujian and its coastal area. *Earthquake* 26 (2), 104–112.
- Sugisaki, R., Takeda, H., Kawabe, I., and Miyazaki, H. (1982). Simplified gas chromatographic analyses of H₂, He, Ar, N and CH₄ in subsurface gases for seismogeological studies. *Chem. Geol.* 36, 217–226. doi:10.1016/0009-2541(82)90048-1
- Teng, J. W., Si, X., Zhuang, Q. X., et al. (2019). Fine structures of crust and mantle and potential hot dry rock beneath the Zhangzhou Basin. *Chin. J. Geophys.* 62 (5), 1613–1632. doi:10.6038/cjg2019L0595
- Tian, J., Li, Y., Zhou, X., Pang, Z., Li, L., Xing, L., et al. (2021a). Geochemical characteristics of hydrothermal volatiles from southeast China and their implications on the tectonic structure controlling heat convection. *Front. Earth Sci.* 9, 1863–4621. doi:10.3389/feart.2021.786051
- Tian, J., Pang, Z. H., Liao, D., and Zhou, X. (2021b). Fluid geochemistry and its implications on the role of deep faults in the genesis of high temperature systems in the eastern edge of the Qinghai Tibet Plateau. *Appl. Geochem.* 131, 105036. doi:10.1016/j.apgeochem.2021.105036
- Torgersen, T., and Stute, M. (2013). “Helium (and other noble gases) as a tool for understanding long timescale groundwater transport,” in *Isotope methods for dating old groundwater* (Vienna, Austria: IAEA), 179–216.
- Wakita, H., Nakamura, K., Kita, I., Fujii, N., and Notsu, K. (1980). Hydrogen release new indicator of fault activity. *Science* 210 (4466), 188–190. doi:10.1126/science.210.4466.188
- Wang, J. H., Sun, F. M., and Zhang, P. R. (1991). Relationship between hydrogen anomaly and seismic activities. *North China Earthq. Sci.* 9.
- Wang, J. Y., and Huang, S. P. (1988). Compilation of heat flow data for continental area of China. *Scientia Geologica Sinica* 2, 196–204.
- Wang, J. Y., and Huang, S. P. (1990). Compilation of heat flow data in the China continental area. *Seismol. Geol.* 12 (4), 351–363.
- Wang, P. Z., Chen, Y. A., Cao, B. T., et al. (1993a). Crust–upper–mantle structure and deep structural setting of Fujian province. *Geol. Fujian* 7 (2), 79–158.
- Wang, X. (2018). *Formation conditions and hydrogeochemical characteristics of geothermal system in typical deep fracture zone along the coast of Guangdong province*. Beijing, China: Thesis of China University of Geosciences.
- Wang, X. B., Xu, S., Chen, J. F., et al. (1993b). Gas composition and helium isotope composition characteristics of hot springs in Tengchong volcanic area. *Chinese Sci. Bull.* 38 (9), 814–817.
- Wang, Xiaofeng, Liu, Quanyou, Liu, Wenhui, Li, Xiaobin, Cheng, Tao, Li, Xiaofu, et al. (2023). Helium accumulation in natural gas systems in Chinese sedimentary basins. *Mar. Petroleum Geol.* 150, 106155. doi:10.1016/j.marpetgeo.2023.106155
- Wang, Y. (1999). A study on mantle heat flow of continental area of China by Helium isotope ratio of the underground fluid. *Acta geosci. sin.* 20, 48–50.
- Wei, S. Y., et al. (1988). The Geothermal activity and the characteristics of geophysics field in continental margin of Fujian province. *Northwest. Seismol. J.* 10 (3), 74–81.

- Wu, Xiaoqi, Dai, Jinxing, Liao, Fengrong, and Huang, Shipeng (2013). Origin and source of CO₂ in natural gas from the eastern Sichuan Basin. *Sci. China Earth Sci.* 56 (8), 1308–1317. doi:10.1007/s11430-013-4601-x
- Xu, Y. C. (1997). Helium isotope distribution of natural gasses and its structural setting. *Earth Sci. Front.* 4 (3), 185–190.
- Xu, Y. C. (1996). The mantle noble gas of natural gases. *Earth Sci. Front.* 3 (3), 63–71.
- Zhang, J., Wang, B. Y., Tang, X. C., Dong, M., and Ai, Y. F. (2018). Temperature structure and dynamic background of crust and mantle beneath the lithosphere of the South China continental margin. *Chin. J. Geophys.* 61 (10), 3917–3932. doi:10.6038/cjg1018L0448
- Zhang, M. L., Guo, Z. F., Xu, S., Barry, P. H., Sano, Y., Zhang, L., et al. (2021). Linking deeply-sourced volatile emissions to plateau growth dynamics in southeastern Tibetan Plateau. *Nat. Commun.* 12 (1), 4157–4210. doi:10.1038/s41467-021-24415-y
- Zhang, P. R., Wang, J. H., and Sun, F. M. (1993). Hydrogen-a sensitive element to predictable earthquake. *Seismol. Geol.* (1), 69–77.
- Zhao, P., Wang, J. Y., Wang, Y. A., and Luo, D. G. (1995). Characteristics of heat production distribution in SE China. *Acta Petrol. Sin.* 11 (3), 292–305.
- Zhou, X. C., Liu, L., Chen, Z., Cui, Y., and Du, J. (2017). Gas geochemistry of the hot spring in the Litang fault zone, Southeast Tibetan Plateau. *Appl. Geochem.* 79, 17–26. doi:10.1016/j.apgeochem.2017.01.022
- Zhou, X. C., Wang, W. C., Chen, Z., Yi, L., Liu, L., Xie, C., et al. (2015). Hot spring gas geochemistry in western sichuan province, China after the wenchuan ms 8.0 earthquake. *Terr. Atmos. Ocean. Sci.* 26 (4), 361–373. doi:10.3319/tao.2015.01.05.01(tt)
- Zhou, X. C., Wang, W. L., Li, L. W., JianMin, H., LanTian, X., ZhongPing, L., et al. (2020). Geochemical features of hot spring gases in the Jinshajiang-Red River fault zone, Southeast Tibetan Plateau. *Acta Petrol. Sin.* 36 (7), 2197–2214. doi:10.18654/1000-0569/2020.07.18
- Zhuan, Q. X. (2015). Exploration and research on geothermal resources in fujian. *Energy Environ.* 1, 2–4.
- Zhuan, Q. X. (2010). *Fujian geothermal research and practice*. Beijing, China: The Geological Publishing House.